Band-edge modification and mid-infrared absorption of co-deposited $Fe_xZn_{1-x}S$ thin films

Nelly-Ann Molland,[1] Zahra Ghadyani,[1] Eric A. Karhu,[1] Stefano Poggio,[2] Mohammadreza Nematollahi,[1] Morten Kildemo,[1] Turid W. Reenaas,[1] Joseph J. BelBruno[2] and Ursula J. Gibson[1,2,*]

[1]*Physics Dept, Norwegian Univ. of Science and Technology, Trondheim, N-7491 Norway*
[2]*Chemistry Dept., Dartmouth College, Hanover NH 03755-6128, USA*
[*]*ursula.gibson@ntnu.no*

Abstract: The bandgap of iron-doped ZnS has been reported by others to change significantly under the addition of a few atomic percent of iron, which would have significant implications for solar energy. Here, thin films of $Fe_xZn_{1-x}S$ with x = 0 to 0.24 were made by co-deposition of Fe and ZnS using thermal evaporation. In contrast to results on nanoparticles and electrodeposited materials, all co-deposited films had optical properties consistent with a direct bandgap of ~3-3.5 eV. The absorption peak at 2.7 μm from substitutional Fe^{2+} in the ZnS films was well isolated up to concentrations of over 2% (~10^{21}cm^{-3}), despite the small crystallite size, suggesting the films may have applications as mid-infrared saturable absorbers. Increasing dopant concentration resulted in band edge softening. Density functional calculations are presented and are consistent with our observations of the Fe:ZnS films, demonstrating spin-polarized midgap states and additional states at the band edge.

OCIS codes: (160.4760) Optical properties; (240.0310) Thin films.

References and links

1. H. Hu and W. Zhang, "Synthesis and properties of transition metals and rare-earth metals doped ZnS nanoparticles," Opt. Mater. **28**(5), 536–550 (2006).
2. C. Tablero, "Correlation effects and electronic properties of Cr-substituted SZn with an intermediate band," J. Chem. Phys. **123**(11), 114709 (2005).
3. P. C. Patel and P. C. Srivastava, "Fe doping in ZnS for realizing nanocrystalline-diluted magnetic semiconductor phase," J. Mater. Sci. **49**(17), 6012–6019 (2014).
4. J. Xie, "First-principles study on the magnetism in ZnS-based diluted magnetic semiconductors," J. Magn. Magn. Mater. **322**(19), L37–L41 (2010).
5. S. Mirov, V. Fedorov, I. Moskalev, M. Mirov, and D. Martyshkin, "Frontiers of mid-infrared lasers based on transition metal doped II–VI semiconductors," J. Lumin. **133**, 268–275 (2013).
6. V. Fedorov, D. Martyshkin, M. Mirov, I. S. Moskalev, S. Vasilyev, J. Peppers, S. B. Mirov, and V. P. Gapontsev, "Fe-doped II-VI Mid-Infrared Laser Materials for the 3 to 8 μm Region," in *CLEO: 2013*, OSA Technical Digest (online) (Optical Society of America, 2013), p. JM4K.2.
7. A. B. Kashyout, A. S. Aricò, G. Monforte, F. Crea, V. Antonucci, and N. Giordano, "Electrochemical deposition of ZnFeS thin film semiconductors on tin oxide substrates," Sol. Energy Mater. Sol. Cells **37**(1), 43–53 (1995).
8. A. Kashyout, A. Arico, N. Giordano, and V. Antonucci, "Influence of Annealing Temperature on the Crystallographic and Optical-Properties of Electrodeposited Znfes Thin-Film Semiconductors," Mater. Chem. Phys. **41**(1), 55–60 (1995).
9. H. C. Ong and R. P. H. Chang, "Optical constants of wurtzite ZnS thin films determined by spectroscopic ellipsometry," Appl. Phys. Lett. **79**(22), 3612–3614 (2001).
10. J. L. Horwood, M. G. Townsend, and A. H. Webster, "Magnetic susceptibility of single-crystal Fe1−xS," J. Solid State Chem. **17**(1-2), 35–42 (1976).
11. C. I. Pearce, R. A. D. Pattrick, and D. J. Vaughan, "Electrical and magnetic properties of sulfides," Rev. Mineral. Geochem. **61**(1), 127–180 (2006).
12. S. S. H. Abdullah, "Optical effect of Fe doped wurtzite ZnS nanoparticles," *Proceedings of the 2nd WSEAS International Conference on Nanotechnology,* 191–194 (2010).

#240246 Received 8 May 2015; revised 11 Jun 2015; accepted 17 Jun 2015; published 23 Jun 2015

13. S. H. Deulkar, C. H. Bhosale, and M. Sharon, "Optical studies on non-stiochiometric (Zn, Fe)S chalcogenide bulk pellets prepared by coprecipitation," Mater. Chem. Phys. **111**(2-3), 260–264 (2008).
14. Q. J. Feng, D. Z. Shen, J. Y. Zhang, Y. M. Lu, Y. C. Liu, and X. W. Fan, "Influence of Fe content on the structural and optical properties of ZnFeS thin films," Mater. Chem. Phys. **96**(1), 158–162 (2006).
15. F. Zhu, S. Dong, and G. Yang, "Ferromagnetic properties in Fe-doped ZnS thin films," Optoelectron. Adv. Mater.-, Rapid Commun. **4**, 2072–2075 (2010).
16. B. K. Li, C. Wang, I. K. Sou, W. K. Ge, and J. N. Wang, "Anomalous photocurrent observed in an Fe–ZnS:Fe Schottky diode," Appl. Phys. Lett. **91**(17), 172104 (2007).
17. Y. A. Nitsuk, Y. A. Vaksman, V. V. Yatsun, and Y. N. Purtov, "Optical absorption and diffusion of iron in ZnS single crystals," Funct. Mater. **19**, 182–186 (2012).
18. K. L. Lewis, G. S. Arthur, and D. A. Edwards, "The incorporation of iron impurities in cubic ZnS," J. Cryst. Growth **59**(1-2), 201–209 (1982).
19. J. H. Zhang, J. W. Ding, J. X. Cao, and Y. L. Zhang, "Infrared, visible and ultraviolet absorptions of transition metal doped ZnS crystals with spin-polarized bands," J. Solid State Chem. **184**(3), 477–480 (2011).
20. M. P. Frolov, Y. V. Korostelin, V. I. Kozlovsky, Y. P. Podmar'kov, S. A. Savinova, and Y. K. Skasyrsky, "3 J pulsed Fe:ZnS laser tunable from 3.44 to 4.19 μm," Laser Phys. Lett. **12**(5), 055001 (2015).
21. M. Nematollahi, X. Yang, L. M. Aas, Z. Ghadyani, M. Kildemo, U. J. Gibson, and T. W. Reenaas, "Molecular beam and pulsed laser deposition of ZnS:Cr for intermediate band solar cells," Sol. Energ. Mat. Sol. Cells (to be published) (2015).
22. R. Swanepoel, "Determination of the thickness and optical-constants of amorphous-silicon," J. Phys. E Sci. Instrum. **16**(12), 1214–1222 (1983).
23. D. Minkov and R. Swanepoel, "Computerization of the optical characterization of a thin dielectric film," Opt. Eng. **32**(12), 3333–3337 (1993).
24. J. D. Dow and D. Redfield, "Toward a unified theory of Urbach's rule and exponential absorption edges," Phys. Rev. B **5**(2), 594–610 (1972).
25. A. Abbad, S. Bentata, H. A. Bentounes, W. Benstaali, and B. Bouadjemi, "Study of electronic and magnetic properties of binary zinc sulfide and ternary manganese- and iron-substituted alloys," Mater. Sci. Semicond. Process. **16**(3), 576–581 (2013).
26. E. J. Baerends, "Precise density-functional method for periodic structures," Phys. Rev. B Condens. Matter **44**(15), 7888–7903 (1991).
27. S. Vosko, L. Wilk, and M. Nusair, "Accurate spin-dependent electron liquid correlation energies for local spin-density calculations - a critical analysis," Can. J. Phys. **58**(8), 1200–1211 (1980).
28. J. P. Perdew, K. Burke, and M. Ernzerhof, "Generalized gradient approximation made simple," Phys. Rev. Lett. **77**(18), 3865–3868 (1996).
29. Y. Okada, N. J. Ekins-Daukes, T. Kita, R. Tamaki, M. Yoshida, A. Pusch, O. Hess, C. C. Phillips, D. J. Farrell, K. Yoshida, N. Ahsan, Y. Shoji, T. Sogabe, and J.-F. Guillemoles, "Intermediate band solar cells: Recent progress and future directions," Appl. Phys. Rev. **2**(2), 021302 (2015).

1. Introduction

Transition-metal doped zinc chalcogenides have been studied extensively for their luminescence properties [1]. Recently, they have been the subject of renewed interest, for production of low-cost, nontoxic solar cells [2], as possible dilute magnetic semiconductors [3,4], and as materials for mid-infrared laser sources [5,6] and saturable absorbers. $Fe_xZn_{1-x}S$ thin films have also been suggested for use in photoconversion as absorbers, due to reported tunability of the band gap and favorable large absorption coefficients [7,8]. Several stable crystal forms exist in the $Fe_xZn_{1-x}S$ system, with widely varying properties. Pyrite (FeS_2) is a semiconductor with a bandgap of 0.95 eV while the bandgap of pure ZnS is 3.5-3.8eV depending on the crystal form and preparation method [9]. FeS is reported to be an antiferromagnetic semiconductor at room temperature [10], but samples may be iron deficient, leading to metallic conductivity [11]. Comparison of different synthesis routes for production of thin films for optical applications is thus important.

Various fabrication techniques, including electrochemical deposition [8], spin-coating of nanoparticles [12], pyrolytic spray deposition [13] metal organic chemical vapor deposition (MOCVD) [14,15], and physical vapor deposition methods such as MBE [16] have been used to make such films. Widely varying properties have been reported, possibly because of the challenges of maintaining phase and chemical purity. In particular, for $Fe_xZn_{1-x}S$ thin films made by electrochemical deposition, reduction of the (assumed indirect) band gap from 3.1 eV to 0.6 eV was reported [8] when increasing x from 0.0 to 0.2. Other reports [7,13,14] also indicated a reduction of bandgap, for both indirect and direct gap models fitted to absorption

#240246 Received 8 May 2015; revised 11 Jun 2015; accepted 17 Jun 2015; published 23 Jun 2015

data. However, Schottky diodes grown by MBE between $Fe_{0.04}Zn_{0.96}S$ and Fe indicated that the doped material was an n-type semiconductor with an estimated direct bandgap of ~3.6eV [16], almost the same as the pure material. Our results support the observation of a nearly constant direct bandgap in the ZnS host under the addition of elemental Fe up to x = 0.16 for vacuum-deposited material. Density functional theory calculations are in good agreement with the observed properties of the films.

In addition to changes in the bandgap, isolated transition metal impurities typically introduce d-electron related absorption. For Fe in crystalline ZnS, there is a strong absorption band at 2.7μm [17,18], of interest for the development of mid-infrared lasers; thin films may allow the development of compact waveguide sources. The presence of a well-defined absorption peak in the infrared is clear evidence of substitutional placement of Fe in the ZnS lattice. The mid-gap states have also been proposed for demonstration of the principle of an intermediate band solar cell [19].

In this paper, we used physical vapor deposition (PVD) for the production of Fe-doped ZnS; both co-deposition from Fe and ZnS sources and co-deposition of FeS and ZnS were performed. The iron sulfide source was used to explore whether formation of FeS during synthesis might explain the inconsistency of previous results. Due to reports of an indirect band gap in Fe:ZnS, which would be associated with crystallographic changes, the structural as well as optical properties were investigated. We found that atomic Fe doping resulted in only a small reduction in a direct bandgap. Films made with the FeS source were absorptive and largely disordered, which supports the conjecture that earlier reports of a reduced bandgap may have been due to the formation of this and other compounds during synthesis. The Fe^{2+} absorption peak in our films at 2.7 μm is well-isolated, with a width and position similar to that of single crystal Fe:ZnS recently used to demonstrate a broadly tuneable mid-IR laser [20].

2. Experimental

Two deposition systems were used in the work described here, one ultrahigh vacuum (UHV) chamber with a base pressure of 4×10^{-9} Torr with turbomolecular and Ti sublimation pumps and a diffusion- pumped (DP), liquid nitrogen trapped system with a base pressure of 2×10^{-6} Torr. Source materials used were Fe (99.98%) and FeS (99.9%) obtained from Sigma Aldrich, and ZnS (99.99%) obtained from Alfa Aesar. In the UHV system, Fe was e-beam evaporated and ZnS was evaporated from a Knudsen cell, whereas in the diffusion-pumped system, ZnS was evaporated from a Mo boat and the Fe and FeS were vaporized using an alumina-coated basket (R.D. Mathis). Substrates were single crystal (100) silicon, UV grade fused silica, IR quartz, CaF_2 and c-plane sapphire. Substrates were sonicated in acetone and isopropanol, and blown dry with nitrogen before loading. Deposition rates for the Fe and FeS sources varied between 0.2 and 1 Å/sec, while ZnS was deposited between 4 and 12 Å/sec. All films were deposited onto room temperature substrates.

Films were characterized by X-ray diffraction (D8 Advance DaVinci from Bruker), and optical spectroscopy over the range 300nm - 4μm (OLIS 14, Bruker Tensor 27). Energy dispersive X-ray spectroscopy (EDS) in a Hitachi TM3000 was used to determine the atomic percentage of Fe in the films and Rutherford Backscattering Spectrometry (1.7 MeV tandem accelerator at Arizona State Univ.) was used to confirm these values. Concentration values given in the paper and shown in the figures are the atomic percentage of Fe in the films (i.e. 10% Fe corresponds to $Fe_{0.2}Zn_{0.8}S$), as all films were found to have a metal:sulfur ratio close to 1. Transmission electron micrographs and diffraction patterns were obtained using a JEOL JEM-ARM200F. Thicknesses were measured with a Tencor alphastep. Films deposited in the DP system were 160-250 nm thick, while those deposited in the UHV system were up to 3.5μm thick.

#240246 Received 8 May 2015; revised 11 Jun 2015; accepted 17 Jun 2015; published 23 Jun 2015

3. Results and discussion

Several reports on the formation of Fe-doped ZnS have used Tauc plot fits to an indirect gap model to determine the change in the bandgap upon the addition of iron. Because a crystal structure change would necessarily accompany the transformation from the direct bandgap of pure ZnS, detailed structural studies were undertaken using X-ray diffraction (Fig. 1) and transmission electron microscopy. The results indicate that only the explicit use of FeS starting material during growth of the films results in any significant alteration in the structure.

3.1 Structure

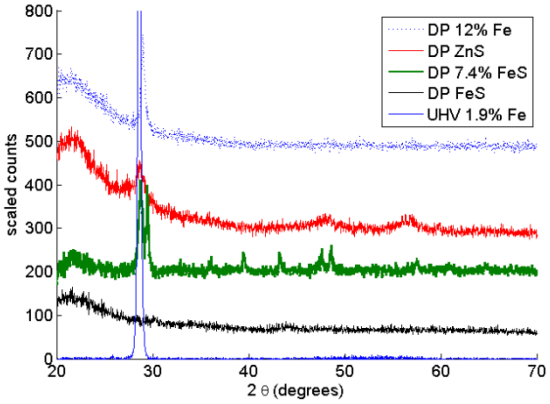

Fig. 1. X-ray diffraction of sample films. From top –films from the diffusion pumped system with iron content 12% (from Fe), 0%(red) and 7.4% (FeS source), a pure FeS film and a 3.5µm thick film with 1.9% Fe deposited in UHV. The amorphous quartz substrate reflection appears at ~22°.

X-ray diffraction and transmission electron microscopy were used to assess phase purity and determine grain size, for comparison with earlier nanoparticle-derived material properties. The full-width half maximum was 0.5-1° for the ZnS and Fe:ZnS film peaks independent of the film thickness or deposition system, implying grain sizes of 10-20 nm (determined using the Debye-Scherrer formula). The broad peak at low angles is from the substrate. The predominant film-related peak was at 28.7°, coincident with both the ZnS (111) cubic (sphaelerite) and (0002) hexagonal (wurtzite) reflections, with additional peaks evident around 47° and 56° that also index to both the hexagonal and cubic forms of ZnS. The small peak at approximately 25.8° in the 3.5 µm thick Fe:ZnS (UHV 1.9%) film is due to CuK_{β} radiation from the non-monochromatic X-ray source. For the films doped with high concentrations of Fe, there was a slight reduction in the lattice constant, consistent with the smaller ionic radius of Fe; e.g. for 12% Fe, the main peak shifted to 29° (~2% reduction). The mixed film made from pre-reacted FeS showed a double peak near 28.7°, suggesting phase separation, while the pure FeS film, which was 38nm thick (to permit optical studies), displayed weak peaks from the (0002) and (200) reflections that match those seen in MOCVD growth [14]. It is clear from the X-ray data that the origin of iron in a doped ZnS film is responsible for significant structural differences. Fe from an atomic source appears to incorporate substitutionally, while FeS as the source leads to a composite, rather than an iron-doped ZnS film.

#240246 Received 8 May 2015; revised 11 Jun 2015; accepted 17 Jun 2015; published 23 Jun 2015

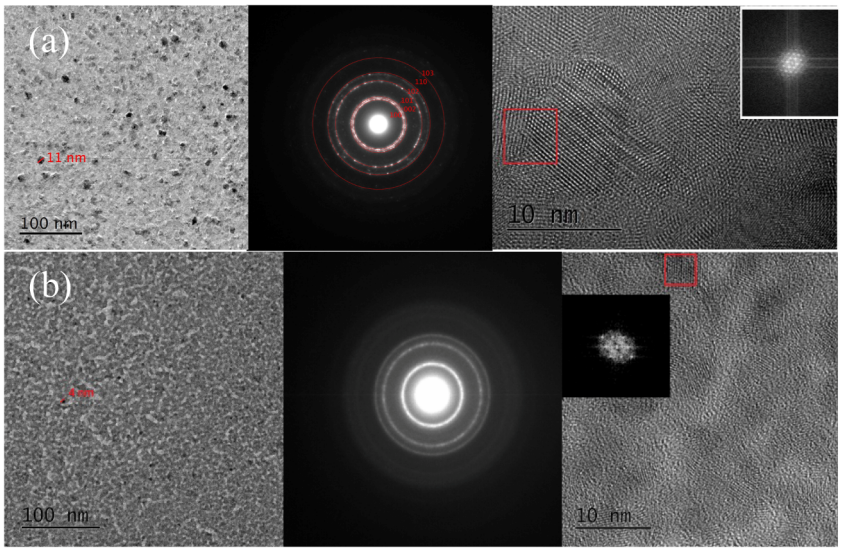

Fig. 2. TEM bright-field micrographs and diffraction images for the a) Fe:ZnS and b) FeS:ZnS films deposited onto carbon grids. Insets are Fourier transforms of the selected regions of the images.

TEM studies were performed on a 73 nm thick film with 6.5% Fe, co-deposited in the DP chamber from elemental Fe and ZnS directly onto a carbon coated TEM grid, with results shown in Fig. 2(a). The film was composed of ~10-20 nm crystalline grains, a value similar to that indicated by XRD results. Electron diffraction patterns from all areas of the film studied showed hexagonal symmetry associated with either the (111) sphaelerite or (002) wurtzite structure. While for pure ZnS films the lateral grain size typically increases to ~500 nm in a micron-thick film [21], SEM (not shown), XRD and TEM studies on our films indicate that the inclusion of even 0.2% transition metal ions in ZnS suppresses grain growth.

TEM studies on a 20 nm thick DP film (3% Fe) deposited from FeS and ZnS showed evidence of crystallinity in only a few small regions (Fig. 2(b)), and the electron diffraction patterns had poorly resolved rings with only slight modulation in the intensity as a function of azimuth. Bright field images suggested possible phase separation in agreement with the X-ray diffraction results. Grain sizes in the film were on the order of 4-5 nm.

3.2 Optical properties

The optical response of the films made in the two vacuum systems was very similar, suggesting that contamination from background gases was not a significant problem in the

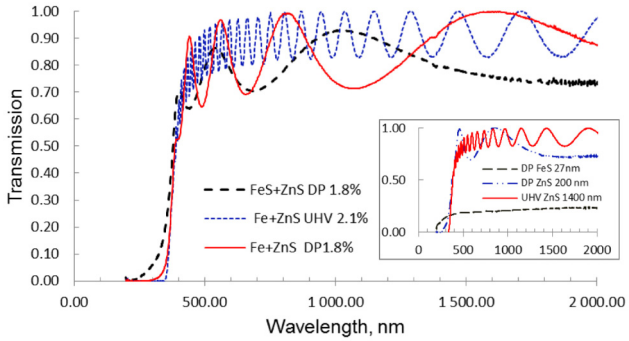

Fig. 3. Optical transmission of selected Fe-doped ZnS films. Inset shows pure ZnS and FeS films.

#240246 Received 8 May 2015; revised 11 Jun 2015; accepted 17 Jun 2015; published 23 Jun 2015

DP chamber. Figure 3 shows the transmission of three films with a low concentration of Fe, made by different methods, measured relative to bare substrates of the type used for each film. The interference fringes are of different amplitudes because the two DP films were deposited on fused silica, while the UHV film was deposited on sapphire, and the higher substrate index reduces the contrast with the film. The closer spacing of the UHV interference fringes is due to the larger thickness of the film. The measured film thicknesses were 337 nm for the DP Fe + ZnS film, 230nm for the DP FeS + ZnS film and 2225 nm for the UHV Fe + ZnS film. The low concentration (2.1% Fe) UHV Fe + ZnS film has the sharpest cutoff and the (thinner) DP Fe + ZnS film shows similar transparency, with a cutoff at 335nm indicating a bandgap of approximately 3.7eV. The film deposited using FeS as a source has increased absorption through the entire visible range, but slightly increased short wavelength transmission, which is attributed to the non-uniform inclusion of iron into the structure and the presence of FeS. The inset shows the transmission for pure ZnS and pure FeS films for comparison. The higher transparency at short wavelengths for the DP deposited ZnS films is partly due to the smaller thickness, but in addition, the grain size in the UHV films increases with large thicknesses and may cause increased scatter.

Samples were analyzed using the Swanepoel [22,23] method to obtain n, k and α values for the materials as a function of energy, and selected films were also analyzed by ellipsometry. Figure 4(a) shows that there was good agreement between the methods and Fig. 4(b) shows a sample Tauc plot using the direct gap model. While the index of refraction remained close to that of pure ZnS, the imaginary part of the refractive index increased upon the addition of

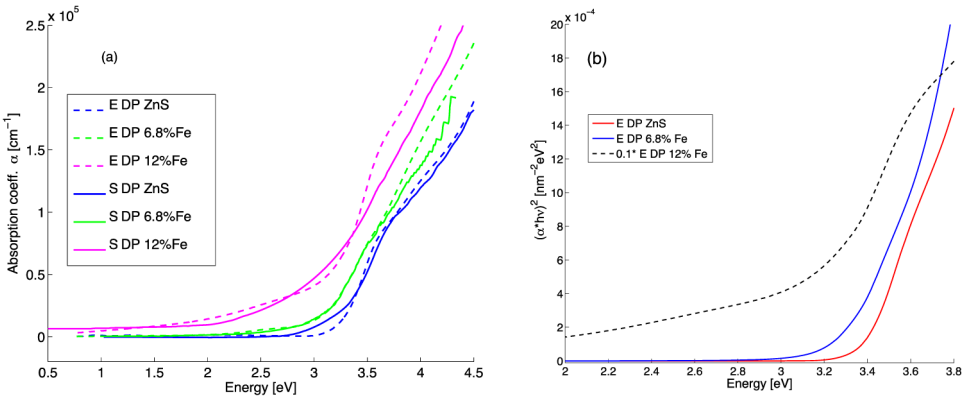

Fig. 4. a)Absorption coefficient for pure ZnS, 6.8% and 12% Fe films, analyzed by ellipsometry (dashed lines-E) and the Swanepoel method (solid lines-S) and b) Tauc plot for these samples, showing increased absorption and softening of the band edge with the addition of iron.

iron, and band edge softening was observed. The most common treatment of such states is to fit the excess absorption to an Urbach model [24], with a dependence given by

$$\alpha(E) = \alpha_0 e^{(E/E_U)} \quad (1)$$

Where α_0 and E_U (the Urbach Energy) are fitting parameters and E is the photon energy. The Urbach energy characterizes the width of the exponential absorption edge. The derived E_U values (Fig. 5(a)) increased upon the addition of iron to the films.

Tauc plots were made to determine the value of the direct bandgap as a function of Fe content and the results are shown in Fig. 5(b). The uncertainties shown in the values of the bangap, E_g, are due to residual curvature in the plots. Other groups [7,8,14] have presented results on similar materials using an indirect gap model, but experimental crystallographic observations and band structure calculations [25] support the existence of a direct bandgap at

#240246 Received 8 May 2015; revised 11 Jun 2015; accepted 17 Jun 2015; published 23 Jun 2015

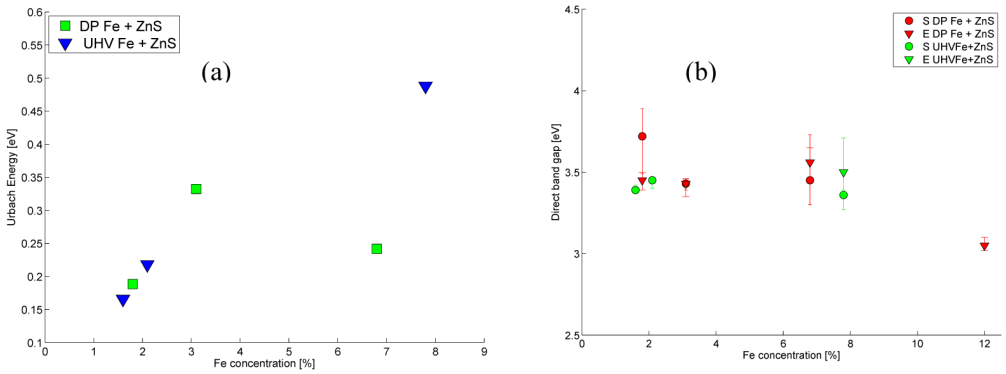

Fig. 5. a) derived Urbach energy and b) band gap, E_g as a function of Fe concentration, as determined from (S) Swanepoel and (E) ellipsometry analysis.

the doping levels used in this study.

Low levels of transition metal doping in ZnS films results in only small changes in the visible optical properties, and in a fine-grained microstructure with reduced short-wavelength scatter. Up to 4% Fe, little change was seen in the values of k in the visible region. However, pronounced absorption was observed in the near infrared, where there is an absorption band at 0.46 eV (3700 cm^{-1},2.7 µm) attributed to Fe^{2+} [5]. Figure 6(a) shows the near infrared absorption coefficient due to the ^5E to $^5T_2$ transition, for a film with 2.1% Fe and a thickness of 3.5 µm. The strong, well-isolated peak suggests that similar films with lower doping levels may be useful as thin film saturable absorbers or possibly as laser gain media for the mid-infrared [6], depending on scattering and lifetime characteristics.

4. Modeling

Density functional theory (DFT) calculations were undertaken to determine the density of states (DOS) for iron substituted for zinc in a crystalline ZnS lattice. While numerical values of the band gap obtained in such a calculation are often underestimates, valuable comparisons can be made between similar structures.

Spin unrestricted DFT calculations were performed using the Amsterdam Density Functional BAND-structure program (BAND 2013 [26]) on a 3x2x2 repetition of the primitive cubic structure ($Zn_{24}S_{24}$). A Zn atom was subsequently substituted with a Fe atom

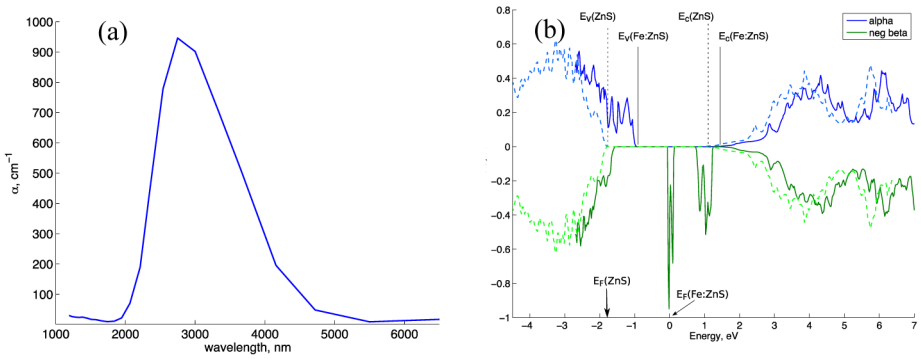

Fig. 6. a) measured absorption in the mid-IR for a film with 2.1% Fe and b) density of states calculated for pure ZnS (dashed lines) and $FeZn_{23}S_{24}$ (solid lines), with green and blue for the two spin states. The energies in the pure ZnS plot are shifted by −1.8eV to allow comparison of the curve shapes. E_v and E_c indicate the valence and conduction band edges and E_F denotes the position of the Fermi level for each material.

#240246 Received 8 May 2015; revised 11 Jun 2015; accepted 17 Jun 2015; published 23 Jun 2015

giving a structure with the chemical composition $FeZn_{23}S_{24}$, corresponding to ~2% Fe. The structures were initially optimized using the Local Density Approximation (LDA) [27]. A second geometry optimization was then performed using the more accurate Perdew-Burke-Ernzerhof (PBE) [28] functional. A double-ζ basis set was used for all atoms. The 3d, 4s and 4p electrons of Zn and Fe were treated as valence electrons in the calculation as were the 3s and 3p electrons of S. The convergence criteria on all simulations were 1.36 x 10^{-2} eV for the energy and 2.7 x 10^{-2} eV/Å for the gradient.

Figure 6(b) shows the band structure calculated for pure ZnS and $FeZn_{23}S_{24}$. To make comparison of the curve shapes easier, the plot for the pure ZnS is shifted by 1.8eV. The positions of the valence band (E_v) and conduction band (E_c) edges are indicated for each of the materials, and the two spin states (denoted alpha and beta) are displayed by multiplying the beta density of states by −1.

The pure ZnS film has a calculated bandgap of 3eV, and the Fermi energy (E_F) lies very close to the valence band edge. When iron is introduced, narrow d-orbital levels due to the Fe ions appear mid-gap, the Fermi energy shifts, and additional, spin polarized states appear near the valence band edge. We identify the valence band edge in Fe:ZnS as shown because the mid-gap states are localized and sparse. With E_F near the lower level associated with the impurity, there is sufficient occupation so that transitions between different energy levels on a single ion can give rise to infrared absorption.

The additional (alpha) states at the valence band edge result in softening of the band edge, in agreement with experimental results, although both the density of states (based on the absorption changes), and the energy range (compared to the observed Urbach energy) are overestimated compared to experiment. The bandgap for the beta states is essentially unchanged from the undoped case.

The modeling is in agreement with the experimental observation of a slightly narrowed gap and ionic mid-gap levels, and supports the observation that the films retain approximately the same bandgap energy as crystalline ZnS. The location of the Fermi level, within the Fe intragap states for the doped material, suggests this as a candidate for demonstration of the intermediate band solar cell concept [29].

5. Conclusion

We find that for elemental Fe added to ZnS, the iron enters the lattice as Fe^{2+}, and introduces additional states at the band edge. It does not change the structure or direct gap of the ZnS at concentrations below 8-10%. Films deposited from a mixture of FeS and ZnS showed very little crystallinity, and had an increased level of absorption, suggesting that the FeS and ZnS formed a near-amorphous composite material with absorption from a variety of Fe binding positions. Prior reports of a widely tunable indirect bandgap are likely due to phase impurity rather the inclusion of iron.

Fe^{2+} absorption with a FWHM of 0.2eV, comparable to that reported in single crystals by Mirov, *et al.* [5], was observed in the near infrared. This suggests that these films may find use as saturable absorbers or possibly as waveguide laser materials and that they warrant further study.

Acknowledgments

This work was supported by a NorTEM seed grant, NoTUR grant NN9291K and NFR contract 219686/O70

#240246 Received 8 May 2015; revised 11 Jun 2015; accepted 17 Jun 2015; published 23 Jun 2015